Original Article

DOI: 10.5582/bst.2024.01044

High-frequency hearing vulnerability associated with the different supporting potential of Hensen's cells: SMART-Seq2 RNA sequencing

Yiding Yu[1,2,3], Yue Li[1,2,3], Cheng Wen[1,2,3], Fengbo Yang[4], Xuemin Chen[5,6], Wenqi Yi[5,6], Lin Deng[1,2,3], Xiaohua Cheng[1,2,3], Ning Yu[5,6,*], Lihui Huang[1,2,3,*]

[1] Otolaryngology Head and Neck Surgery, Beijing Tongren Hospital, Capital Medical University, Beijing, China;
[2] Beijing Institute of Otolaryngology, Beijing, China;
[3] Key Laboratory of Otolaryngology Head and Neck Surgery, Ministry of Education, Beijing, China;
[4] Otolaryngology Head and Neck Surgery, Affiliated Hospital of North Sichuan Medical College, Nanchong, China
[5] College of Otolaryngology Head and Neck Surgery, Chinese PLA General Hospital, Beijing, China;
[6] National Clinical Research Center for Otolaryngologic Diseases, Beijing, China.

SUMMARY Hearing loss is the third most prevalent physical condition affecting communication, well-being, and healthcare costs. Sensorineural hearing loss often occurs first in the high-frequency region (basal turn), then towards the low-frequency region (apical turn). However, the mechanism is still unclear. Supporting cells play a critical role in the maintenance of normal cochlear function. The function and supporting capacity of these cells may be different from different frequency regions. Hensen's cells are one of the unique supporting cell types characterized by lipid droplets (LDs) in the cytoplasm. Here, we investigated the morphological and gene expression differences of Hensen's cells along the cochlear axis. We observed a gradient change in the morphological characteristics of Hensen's cells along the cochlear tonotopic axis, with larger and more abundant LDs observed in apical Hensen's cells. Smart-seq2 RNA-seq revealed differentially expressed genes (DEGs) between apical and basal Hensen's cells that clustered in several pathways, including unsaturated fatty acid biosynthesis, cholesterol metabolism, and fatty acid catabolism, which are associated with different energy storage capacities and metabolic potential. These findings suggest potential differences in lipid metabolism and oxidative energy supply between apical and basal Hensen's cells, which is consistent with the morphological differences of Hensen's cells. We also found differential expression patterns of candidate genes associated with hereditary hearing loss (HHL), noise-induced hearing loss (NIHL), and age-related hearing loss (ARHL). These findings indicate functional heterogeneity of SCs along the cochlear axis, contribute to our understanding of cochlear physiology and provide molecular basis evidence for future studies of hearing loss.

Keywords cochlea, Hensen's cells, lipid droplets, RNA sequencing

1. Introduction

The cochlea is a very sophisticated 3D structure. The Organ Corti is a highly specialized hearing organ located within the cochlea that is comprised of hair cells (HCs) and their adjacent supporting cells (SCs). Both HCs and SCs are essential for normal hearing, acting as primary structures for sound perception (*1-3*). Within the cochlea, HCs and SCs form an ordered asymmetrical pattern, extending from the basal to the apical axis. SCs provide the necessary metabolic and electrolyte environment for HCs to maintain their normal physiological functions and form the supporting Corti apparatus structure (*4,5*). The SCs can be identified as several types: Hensen, Deiter, internal and external Pillar, Boettcher, and Claudius cell. Hensen's cells, a type of SC found on the basement membrane's outer side, are notable for their lipid droplets (LDs) enrichment. Hensen's cells can be individually identified in the cochlea of guinea pigs due to the LDs in the cytoplasm (*1,6*). More studies have shown that Hensen's cells may have some other important functions such as the regulation of sensory cell differentiation and development, maintenance of a stable ionic state, modulation of sensorimotor function, and development of synaptogenesis (*7-12*).

Smart-seq2 is a single-cell RNA sequencing

technology that enables the extraction and sequencing of RNA from individual cells or cell masses, and we took this approach specifically to examine only pure Hensen's cells to avoid the influence of other parts of the cochlea on the result. We observed a gradient enrichment of LDs in Hensen's cells along the tonotopic axis. Analysis of differentially expressed genes (DEGs) suggests that these disparities might be linked to variations in energy storage and metabolic capacities. Following sonic induction, the low-frequency region (apical turn) recovers faster from the noise stimuli than the high-frequency region (basal turn). The increased vulnerability of high-frequency hearing may be related to the lower "supporting ability and potential" of the Hensen's cells from the basal turn.

2. Materials and Methods

2.1. Animals

Five-week-old healthy adult male albino guinea pigs weighing 230 g were used for this study. The animals were purchased from Vital River Laboratory Animal Technology Co., Ltd. (Beijing, China). The study's animal care and use protocols received approval from the Chinese Capital Medical University's Institutional Animal Care and Use Committee.

2.2. Immunofluorescence

The cochleae were transferred into an Eppendorf tube containing paraformaldehyde and kept overnight at 4 °C. A 10% EDTA solution (Solarbio, China) was used for decalcification at room temperature for 7 days. The sensory epithelium of every turn was dissected out and stained with BODIPY 493/503 (Invitrogen, Cat# D3922, 1:200) for 2 h without light to display the LDs. Then, the sections were rinsed with 0.1 M PBS three times for 5 min each time and drawn onto a glass slide by using a pipette. The slides were carefully covered with Antifade Mounting Medium (Beyotime, Cat# P0131, China). A confocal microscope (Zeiss, Germany) was used to observe the experimental results.

2.3. Frozen sections and oil red O staining

After decalcification with disodium EDTA for 7 days, the cochleae were dehydrated with 15% and 30% sucrose for 1.5 h each and embedded in optimal cutting temperature compound (Sakura, Cat#4583, Japan) overnight at 4°C. Modiolar sections with a thickness of 10 μm were cut, air dried, fixed in formalin, briefly washed with running tap water for 5 min, and then rinsed with 60% isopropanol. The slides were stained with freshly prepared Oil Red O working solution for 15 min and rinsed with 60% isopropanol. The nuclei were lightly stained with 5 dips in alum hematoxylin and rinsed with distilled water. The slides were mounted in glycerine jelly. A microscope (Zeiss, Germany) was used to observe the samples.

2.4. Dissection and isolation of Hensen's cells

Following anesthesia with pentobarbital sodium (50 mg/kg intraperitoneal injection), guinea pigs were killed by cervical dislocation. The bulla was removed, and the cochlea was exposed. Then, the volute was removed from the basal to the apical turn. Micro tweezers were used to mechanically detach the Hensen's cells from the cochlear basement membrane. A microsyringe was used to transfer the Hensen's cell mass to a 1 ml Eppendorf (EP) tube with 500 μL of extracellular fluid (pH 7.35 and 300 mOsm) and 500 μg of trypsin (Gibco, United States) for digestion. After 10 min of incubation at room temperature, 200 μl of extracellular fluid was added to the EP tube to terminate digestion and gently blown with a pipette gun to digest the tissue into single cells and cell masses. The cell masses were transferred to a new plastic chamber containing an enzyme-free culture medium. Hensen's cells were separated after gentle trituration of the tissue with a small pipette and observed under an inverted microscope (Leica, Germany). One guinea pig was used to collect 2 cell masses from apical and basal turns separately, and three guinea pigs were used for three biological repeats.

2.5. Collection of isolated Hensen's cells

Two glass pipettes pulled by an electrode puller (Narishige, Japan), 70-100 μm in diameter, were used to collect solitary Hensen's cells separately to prevent contamination. These pipettes were mounted in two separate electrode holders on two micromanipulators (Narishige, Japan). A 1 mL syringe was connected to the suction port of the pipette to aspirate or expel the cells. The Hensen's cells were identified based on their specific morphological features. Cells from the apical and basal turns were collected separately in different EP tubes, and stored on ice. Each sample contained 10-15 identified Hensen's cells. All samples were from three animals. Only the identified HCs were aspirated into the first glass micropipette and expelled into the Bovine Serum Albumin (BSA) on the adjacent coverslip for washing. Washed cells were transferred using another clean glass micropipette and expelled into a 0.2 mL thin-walled PCR tube containing 2 μl of a mild hypotonic lysis buffer composed of 0.2% Triton X-100 (Sigma, United States) and 2 U/μL RNase inhibitor (Clontech, Canada).

2.6. Library preparation and RNA sequencing

We followed the Smart-Seq2 protocol for reverse transcription with a few modifications (*13,14*). The library was prepared by using the Smart-Seq v4 Ultra Low Input RNA Kit (Clontech Laboratories, Canada) and Nextera Library Preparation Kit (Illumina, Canada).

The concentration of total extracted RNA from cells ranged from 5 to 10 ng/μL. Subsequently, amplified samples were purified and selected with AMpure XP beads (Beckman, United States). The DNA quality was examined using an Agilent 2100 BioAnalyzer system (Agilent Technologies, CA, United States). The libraries were multiplexed and sequenced on an Illumina X-Ten platform to generate 100-bp paired-end reads. The files from the multiplexed RNA-seq samples were demultiplexed, and fastq files representing each library were generated.

2.7. Data analysis

The low-quality reads were filtered, and the linker sequence was trimmed to obtain clean reads by Trimmomatic (v0.39). Then, STAR (2.7.5c) was utilized to align the reads to the guinea pig reference genome (Cavpor3.0). The reads aligned to genes were counted by cufflinks (v2.2.1). The fragments per kilobase of transcript per million mapped reads (FPKM) values were normalized by cuffnorm, and the gene expression levels were calculated by cuffdiff. The resulting P values were adjusted using Benjamini and Hochberg's approach for controlling the false discovery rate. Significant DEGs were identified with threshold P values < 0.05 and fold-change > 1.2. The DESeq R package was used to conduct differential expression analysis of the two groups, with three biological replicates per condition. Gene Ontology (GO) enrichment analysis was performed using TopGO (v2.24.0), Kyoto Encyclopedia of Genes and Genomes (KEGG) enrichment analysis was performed using DAVID (v6.8), and the results were visualized using ClusterProfiler and ggplot2 package in R (v4.3.1).

3. Results

3.1. Morphological differences between apical and basal turn Hensen's cells.

The presence of LDs is one of the main features of Hensen cells and can be easily identified from the cochlea epithelium. The Hensen's cells were distributed in the outer part of the Corti organ, and those from different turns had different morphologies, especially regarding the volume of LDs. We observed a larger cell body and a greater volume of LDs in the apical turn compared to that in the basal turn (Figure 1A-E). Oil Red O staining's longitudinal observations corroborated the LD distribution patterns across various turns: the LDs were dyed red, and the apical LDs were larger (Figure 2A-F). At the same time, the cochlea basilar membrane from different turns showed that the size and number of LDs decreased along the longitudinal cochlea toward the basal turn, and became unobservable (especially the basal turn) (Figure 1E).

3.2. Analysis of gene expression profiles.

The reads containing adapters or multiple unidentifiable nucleotides and low-quality reads were deleted from the raw reads to obtain clean data (FPKM ≥ 0.5). 1389 DEGs between apical and basal Hensen's cells were identified, 567/1389 (40.8%) DEGs were upregulated in apical cells, while 822/1389 (59.2%) DEGs were upregulated in basal cells (Figure 3A). The heatmap and PCA plot compared the gene expression of six samples from different turns and showed that the six samples from the apical turn and the basal turn could be clustered

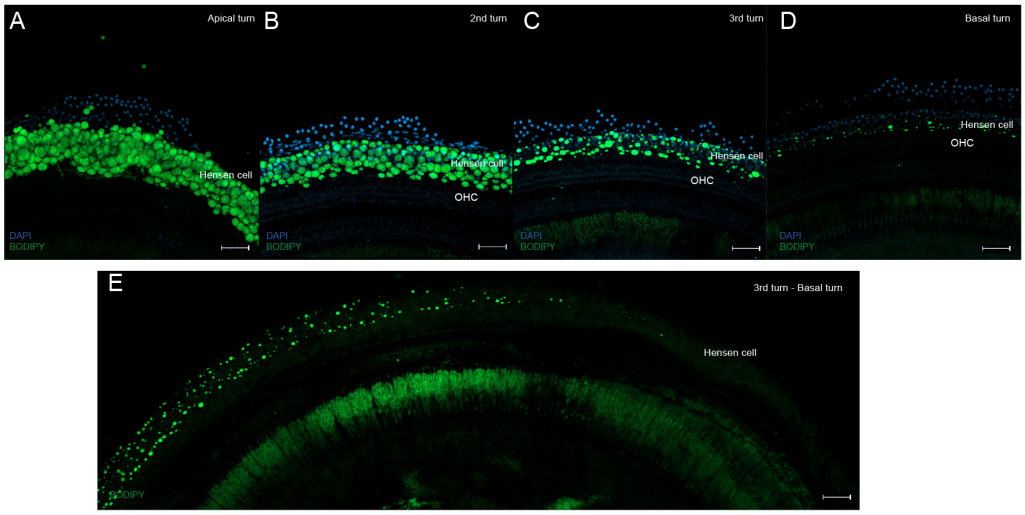

Figure 1. Morphological characteristics of Hensen's cells and the LDs in different turns. A-D: Confocal images scanned on the surface of each turn; green represents the LDs stained by BODIPY, and blue represents cell nuclei stained by DAPI. **E**: LDs gradually become smaller until they disappear. Green represents the LDs stained by BODIPY. The size of the LDs decreases along the longitudinal cochlea apical toward the basal turn, becoming progressively unobservable. Scale bars = 50 μm (apply to A-E). HC: Hair Cell.

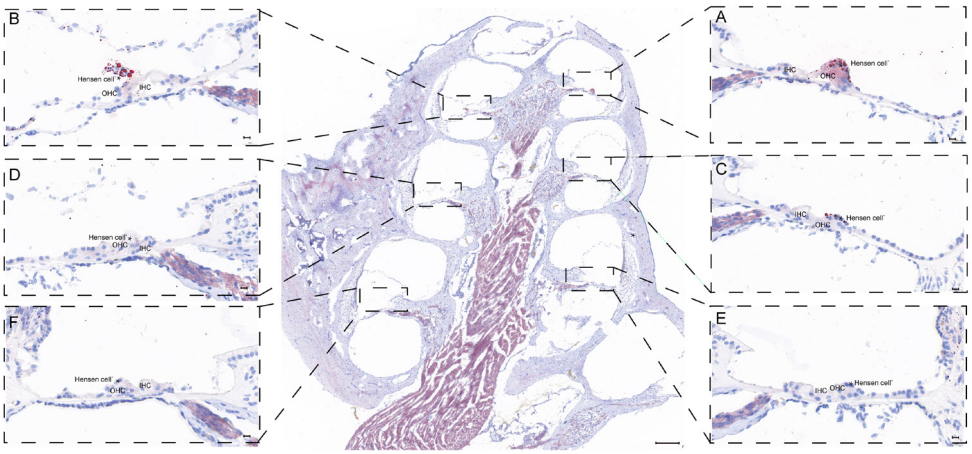

Figure 2. Longitudinal observation of the distribution of LDs in different turns. Oil Red O staining of whole frozen cochlear sections. **A-F**: Oil Red O staining of each turn; red represents the LDs. Longitudinal observation of the distribution of different turns of LDs confirmed the distribution characteristics of LDs, the apical turn enrichs more LDs.**.** Scale bars = 200 μm in the whole cochlea; scale bars = 20 μm in **A-F**. HC: Hair Cell.

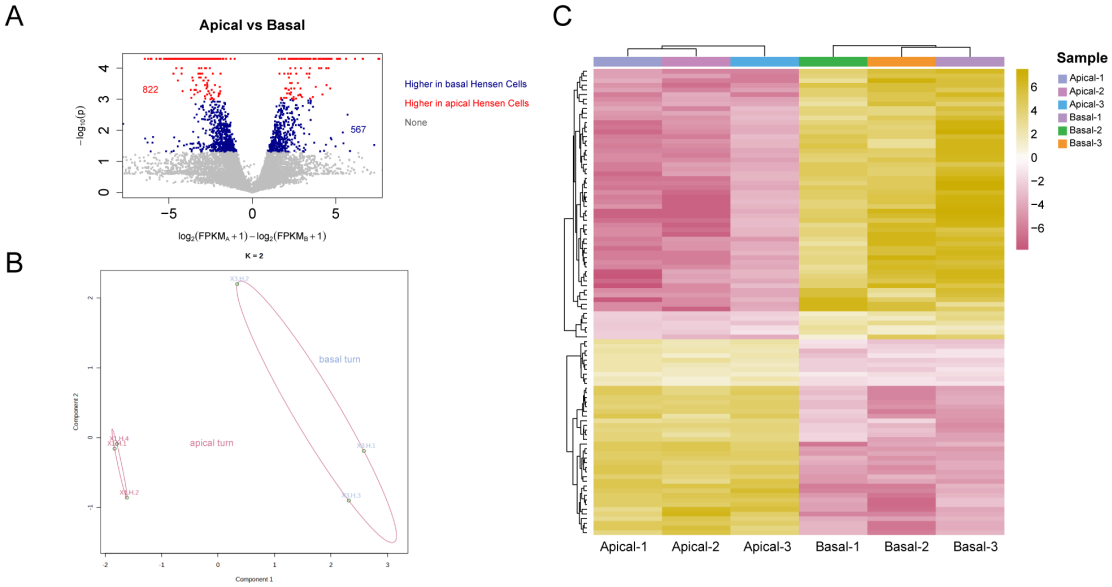

Figure 3. Analysis of DEGs between apical and basal Hensen's cells. A: Volcano plot with the red and blue dots representing the up- and downregulation of differentially expressed genes, respectively. **B**: K-means clustering shows that the samples from the apical and basal turns can be clustered together. **C**: Heatmap generated by the clustering analysis of DEGs and samples. The samples from the apical turn and basal turn could be clustered into two groups, and Hensen's cells from the same site had similar expression patterns.

into two groups, indicating different transcriptional profiles between apical and basal Hensen's cells (Figure 3B, C).

3.3. GO enrichment analysis

The ontology covers three domains: molecular function (MF), cellular component (CC), and biological process (BP). We summarized some of the most significantly enriched GO terms from our analysis, revealing that the DEGs were predominantly associated with the CC, such as extracellular exosome, peroxisomes, and lipid biosynthesis proteins. In terms of MF, the DEGs were significantly involved in processes and functions critical for cellular energy management and metabolic regulation, including activities related to ion transport *via* ATPase activity, redox reactions *via* oxidoreductases, and lipid metabolism *via* fatty acid-CoA ligase activity and lipid transporter activity. In addition, these DEGs played critical roles in metabolic pathways, particularly in lipid oxidation, fatty acid metabolism, and response to decreased oxygen levels. These findings highlight the essential functions of the genes in lipid metabolism and their impact on the cellular antioxidant system, which may affect the cell's ability to maintain redox homeostasis (Figure 4A).

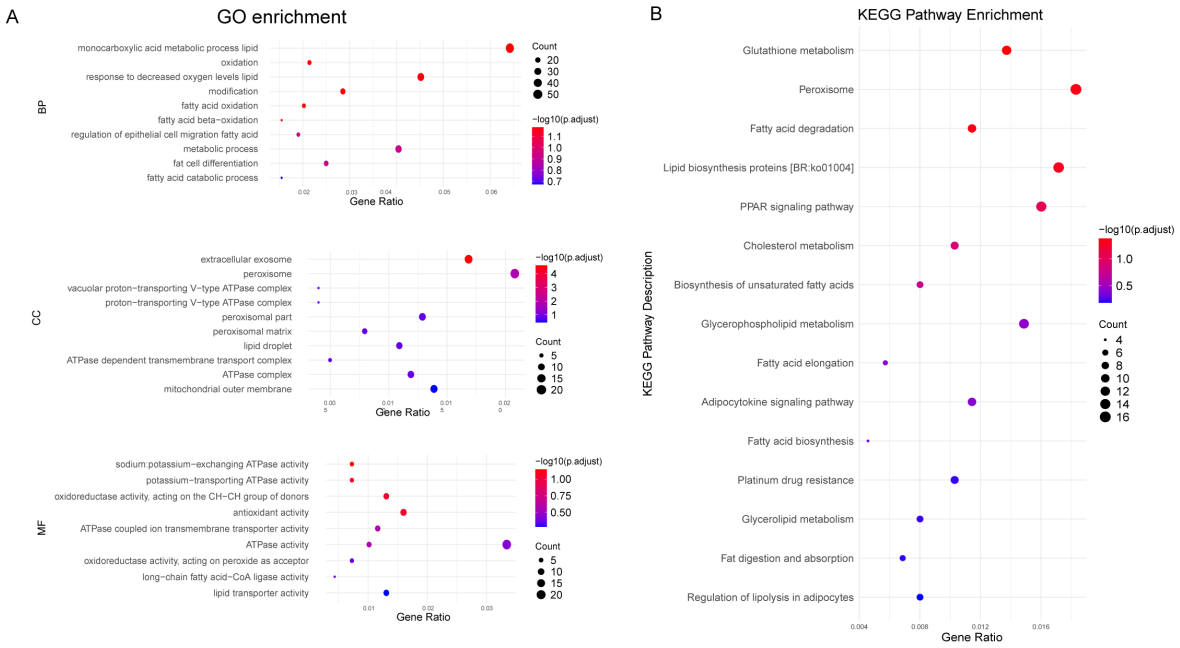

Figure 4. GO bar chart showing significant accumulation and significant KEGG enrichment scatter. A: GO bar chart showing significant accumulation: significantly enriched GO terms based on $p \leq 0.05$; the horizontal axis shows the logarithm of the p value, the vertical axis shows the GO terms, BP terms are shown in green, CC terms are shown in orange, MF terms are shown in blue. **B**: Each dot represents a KEGG pathway; the names of the pathways are shown on the vertical axis, and enrichment factors are shown on the horizontal axis. The larger the enrichment factor is, the more reliable the significant enrichment of the DEGs in the pathway. Both the GO and KEGG enrichment analyses showed that the different pathways between the two groups may be associated with lipid metabolism and oxidative energy supply.

3.4. KEGG enrichment analysis

KEGG pathway analysis revealed a cluster of key pathways that are central to lipid homeostasis and energy balance within Hensen's cell. These pathways range from fatty acid degradation and biosynthesis, including the critical involvement of peroxisomes, to the regulation of these processes by the PPAR signaling pathway. In addition, cholesterol metabolism and unsaturated fatty acid biosynthesis indicate a complex interplay in lipid management. Glycerophospholipid metabolism and the adipocytokine signaling pathway suggest a link between lipid storage and signaling mechanisms. These pathways also emphasize the cellular focus on the regulation of energy storage and utilization, as demonstrated in the pathways for fat digestion and absorption, and regulation of lipolysis in adipocytes. In addition, glutathione metabolism indicates a link to the antioxidant defense system, highlighting the multiple roles of these genes in cellular metabolism (Figure 4B).

3.5. Expression of HHL, NIHL, and ARHL candidate genes

3.5.1. HHL Genes

Mutations in deafness-related genes have been linked to inherited syndromic or non-syndromic hearing loss, and the mutations affect different hearing phenotypes. Therefore, we analyzed the expression of deafness-related genes. Many of these deafness-related genes can be expressed in SCs, and some exclusively in SCs. We compared 36 deafness-related genes (3 of these genes were not found in our samples) that may be expressed in Hensen's cells (*15*). At least 16 of these genes differed in expression by 2-fold or more (|log2FC|>1); among them, *GJB2 and P2RX2* were significantly more highly expressed in the apical turn, and only *COL11A1* was more highly expressed in the basal turn (FDR q-value < 0.05) (Table 1).

3.5.2. Candidate NIHL susceptibility genes

There is increasing evidence that genetic factors may increase susceptibility to noise-induced hearing loss (NIHL), and by conducting a review of previous studies, we compiled a list of some of the genes that may contribute to increased noise sensitivity and compared the expression of these genes in Hensen's cells at different locations. A total of 47 possible NIHL susceptibility genes (*16*) were compared; 7 of these genes were not detected in our samples, and the expression of 25 genes differed 2-fold or more (|log2FC|>1), including 11 genes with higher expression in the apical turn, 1 with a significant difference, and 14 genes with higher expression in the basal turn, 2 with significant differences (FDR q-value < 0.05) (Table 2).

Table 1. Summary of deafness genes that differ between apical and basal Hensen's cells

NO.	Gene Symbol	Apical (FPKM)	Basal (FPKM)	log2 FC	*FDR q*-value	
1	*GJB2*	875.50	43.73	-4.41	0.003*	
2	*P2RX2*	353.00	19.64	-4.25	0.003*	
3	*COL11A1*	2.66	41.62	3.88	0.021*	
4	*GJB6*	99.85	16.33	-2.69	0.150	
5	*WFS1*	50.93	18.04	-1.58	0.170	
6	*SMPX*	604.61	6.60	-6.60	0.474	
7	*EYA4*	4.37	11.99	1.37	0.491	
8	*CIB2*	46.08	23.02	-1.08	0.508	
9	*ILDR1*	15.27	5.76	-1.49	0.513	
10	*TMPRSS3*	28.43	1.81	-4.05	0.527	
11	*ELMOD3*	1.44	10.22	2.75	0.569	
12	*SYNE4*	17.93	4.84	-1.97	0.572	
13	*SOX10*	46.41	22.05	-1.15	0.614	
14	*TPRN*	7.11	2.11	-1.82	0.655	
15	*KARS*	61.08	98.88	0.61	0.694	
16	*MYH9*	18.27	13.37	-0.53	0.716	
17	*CLPP*	17.09	27.47	0.60	0.727	
18	*CLDN14*	8.07	3.38	-1.33	0.733	
19	*EDN3*	0.01	13.99	10.30	0.750	
20	*MSRB3*	7.72	1.57	-2.38	0.759	
21	*TRIOBP*	17.52	11.97	-0.63	0.824	
22	*PNPT1*	18.98	17.51	-0.20	0.889	
23	*GPSM2*	8.38	6.99	-0.35	0.940	
24	*TJP2*	16.68	18.89	0.10	0.941	
25	*CCDC50*	13.14	16.26	0.22	0.958	
26	*COL11A2*	2.04	2.15	0.00	0.997	
27	*EYA1*	45.72	48.71	0.01	0.997	
28	*ESRRB*	0.00	0.00	0.00	1.000	Not detected
29	*ADCY1*	0.00	0.00	0.00	1.000	Not detected
30	*CEACAM16*	0.00	0.00	0.00	1.000	Not detected
31	*GRXCR1*	0.29	0.07	-2.09	1.000	
32	*LHFPL5*	0.10	0.46	2.06	1.000	
33	*MYH14*	0.74	0.00	-7.31	1.000	
34	*OTOGL*	0.90	0.24	-1.95	1.000	
35	*TMC1*	0.05	0.25	2.29	1.000	
36	*TMIE*	0.12	0.17	0.36	1.000	

FPKM: Fragments per kilobase of transcript per million mapped reads. *q-value < 0.05

3.5.3. Candidate ARHL-associated genes

Similarly, we conducted a literature survey and summary of the studies related to pathogenic genes associated with ARHL, focusing on genes that may be mainly expressed in SCs, including *CDH23, CEP104, DCLK, ERBB3, EYA4, GJB2, GRHL2, GRM7, ILDR1, ISG20, KCNQ4, KCNQ5, P2RX2, PCDH20, SLC28A3,* and *TRIOBP* (*17-22*). Some of these candidate genes were not detected in our samples, such as *SLC28A3, KCNQ4, KCNQ5,* and *PCDH20* (FPKM ≤ 0.5). The expression of 7 genes differed 2-fold or more (|log2FC|>1) in different groups, among which 3 were highly expressed in the apical turn, 2 with significant differences (FDR *q*-value < 0.05), and 4 had higher expression in the basal turn, none with a significant difference (Table 3).

4. Discussion

SCs are involved in ionic circulation, structural support, and repair in the inner ear, similar to glial cells for neuronal cells, including the provision of mechanical and nutritional support for HCs (*4,5*). The inherent challenges posed by the deep location and limited quantity of cochlear cells limit research investigating gene expression in cochlear SCs. Most previous studies on cochlear cells have inevitably mixed a variety of different cell types, and potentially important information may be lost in the context of data on complex SC populations (*23-25*). One of the biggest difficulties is obtaining enough cells of one single cochlear type for sequencing. Smart-seq2 RNA sequencing technology has provided new ideas and methods to construct libraries from very small amounts of cells and obtain full-length RNA sequencing (*1,13,14,26-28*). As far as we know, there have been no RNA studies have been conducted using pure Hensen's Cells, this is the first data to investigate the difference between apical and basal Hensen's cells using SMART-seq2 RNA sequencing.

4.1. The morphological differences implied that Hensen's cells have different energy storage capacities and metabolic potential

Table 2. Summary of candidate NIHL-related genes that differ between apical and basal Hensen's cells

NO.	Gene Symbol	Apical (FPKM)	Basal (FPKM)	log2 FC	*FDR q*-value	
1	*GJB2*	814.75	44.35	-4.41	0.003*	
2	*ITGA8*	9.52	103.38	3.84	0.003*	
3	*SLC12A4*	1.63	22.42	3.36	0.020*	
4	*GJB6*	112.94	21.58	-2.69	0.150	
5	*ATP2B2*	18.68	4.57	-2.42	0.204	
6	*GAPDH*	2406.65	1182.68	-1.37	0.336	
7	*CAT*	34.48	80.23	1.11	0.348	
8	*SOD2*	123.31	350.11	1.19	0.403	
9	*PER1*	4.19	14.82	1.92	0.409	
10	*KCNQ1*	35.90	8.48	-1.97	0.434	
11	*SIK3*	11.25	26.95	1.20	0.470	
12	*EYA4*	4.01	15.98	1.37	0.491	
13	*SOD1*	3433.96	2187.52	-0.84	0.525	
14	*HDAC2*	28.34	45.42	0.85	0.565	
15	*NRN1*	0.13	97.16	10.45	0.588	
16	*KCNE1*	9.47	132.04	4.43	0.603	
17	*GRM7*	0.01	6.26	9.81	0.635	
18	*NOTCH1*	7.66	0.97	-3.15	0.645	
19	*DNMT1*	0.61	2.22	2.66	0.656	
20	*CDH23*	0.02	1.60	6.02	0.705	
21	*OGG1*	1.06	5.08	1.66	0.705	
22	*KCNJ10*	1.14	0.40	-2.13	0.743	
23	*PON2*	46.28	62.41	0.31	0.793	
24	*WHRN*	2.13	0.55	-2.02	0.798	
25	*CASP3*	1.78	5.68	1.81	0.814	
26	*FOXO3*	13.63	11.57	0.30	0.819	
27	*NCL*	83.30	91.37	0.25	0.843	
28	*MAPK8*	2.81	2.67	-0.73	0.848	
29	*XRCC1*	9.31	14.21	0.46	0.853	
30	*NFE2L2*	55.98	83.58	0.15	0.897	
31	*UBAC2*	13.45	14.60	-0.20	0.903	
32	*GRHL2*	1.48	1.71	-0.50	0.914	
33	*DNMT3A*	21.61	12.26	-0.17	0.920	
34	*AUTS2*	18.13	14.54	-0.12	0.933	
35	*APEX1*	9.01	10.75	0.18	0.942	
36	*MAPK1*	38.32	42.46	-0.06	0.955	
37	*DFNA5*	0.16	0.05	-3.69	1.000	
38	*FAS*	0.00	0.00	0.00	1.000	Not detected
39	*GJB3*	0.00	0.00	0.00	1.000	Not detected
40	*GJB4*	0.00	0.00	0.00	1.000	Not detected
41	*HSPA1L*	1.03	0.24	-2.22	1.000	
42	*KCNMA1*	0.00	0.00	0.00	1.000	Not detected
43	*KCNQ4*	0.00	0.00	0.00	1.000	Not detected
44	*MYH14*	0.71	0.01	-7.31	1.000	
45	*NOX3*	0.00	0.00	0.00	1.000	Not detected
46	*PCDH15*	0.00	0.00	0.00	1.000	Not detected
47	*POU4F3*	0.39	0.13	-0.21	1.000	

FPKM: Fragments per kilobase of transcript per million mapped reads. *q-value < 0.05

Our morphological analysis showed that cell size and LD size were consistent with a gradual decrease from the apical to the basal turn, especially the gradual disappearance near the basal turn (Figure 1E), which was also confirmed by oil red O staining of frozen sections (Figure 2 A-E). In previous studies, LDs have been considered dynamic lipid storage organelles that respond to external stimuli, participate in a variety of metabolic processes, and are involved in maintaining a relatively stable morphological equilibrium They may not only be composed of lipids, but also contain steroids and various proteins that are thought to play important roles in energy metabolism, protein synthesis, and other biological processes, and may regulate relevant cellular signaling pathways (*29,30*). As seen in the structure of the enriched LDs of Hensen's cells, the cells may have a high energy supply capacity and play an important role in the nutritional support of sensory cells. (*31,32*). In the 1980s, Merchan and his team suggested a possible role for Hensen's cell in hearing. Using a scanning electron microscope, they observed that Hensen's cells showed a partial loss of the plasma membrane to form vacuoles. They hypothesized that cytoplasmic material might be extruded through the vacuoles into the endolymph (*33*). Further studies have described that high-intensity noise exposure resulted in the secretion of LDs from Hensen's

Table 3. Summary of candidate ARHL-related genes that differ between apical and basal Hensen's cells

NO.	Gene Symbol	Apical (FPKM)	Basal (FPKM)	log2 FC	*FDR q*-value	
1	*GJB2*	875.50	44.35	-4.41	0.003*	
2	*P2RX2*	353.00	43.73	-4.25	0.003*	
3	*EYA4*	4.37	19.64	1.37	0.491	
4	*ILDR1*	15.27	11.99	-1.49	0.513	
5	*GRM7*	0.01	5.76	9.81	0.635	
6	*DCLK1*	0.00	9.29	11.16	0.645	
7	*CDH23*	0.02	10.53	6.02	0.705	
8	*CEP104*	2.87	1.20	0.66	0.790	
9	*TRIOBP*	17.52	4.80	-0.63	0.824	
10	*ISG20*	5.36	11.97	0.80	0.863	
11	*GRHL2*	1.72	9.80	-0.50	0.914	
12	*ERBB3*	19.01	1.28	0.13	0.924	
13	*SLC28A3*	0.00	21.94	0.51	1.000	Not detected
14	*KCNQ5*	0.00	0.00	0.00	1.000	Not detected
15	*KCNQ4*	0.00	0.00	0.00	1.000	Not detected
16	*PCDH20*	0.00	0.00	0.00	1.000	Not detected

FPKM: Fragments per kilobase of transcript per million mapped reads. *q-value < 0.05

cells into the endolymphatic space in the guinea pig cochlea. (*34,35*). From the different volumes of the LDs, we can see that the large volume LDs of the apical Hensen's cells have more energy storage potential than those in the basal turn.

Our analysis delved into the gene expression of Hensen's cells from different turns and revealed that DEGs were predominantly enriched in biological processes such as lipid and fatty acid oxidation, along with monocarboxylic acid cycle metabolism. At the same time, pathways involved regulation of lipolysis in adipocytes, fat digestion and absorption, and PPAR signaling were also highlighted (Figure 4B). These patterns suggest that Hensen's cells not only exhibit marked differences in the distribution and volume of LDs but also in the expression of genes involved in lipid synthesis and metabolism. This observation implied that LDs function beyond mere energy reserves; they may also be underpinned by a sophisticated gene regulatory framework poised for rapid adaptive responses to stimuli such as noise and pharmacological agents.

The specific causes of the differences in the distribution of LDs in cells at different turns and whether they exhibit differential gene expression are still not well known. We found a variety of lipid metabolism-related genes were differentially expressed, such as *DGAT2, HACD3,* and *ACOT7*. Among them, the diacylglycerol acyltransferase (*DGAT2*) apical–basal expressed significantly differed, and the gene expression level was 477-fold higher (|log2FC|=8.90) in the apical turn than in the basal turn. *DGAT* is a glycerol-restricted transferase with two isoforms, *DGAT1* and *DGAT2*. *DGAT1* is mainly responsible for the synthesis of triacylglycerol during fat absorption and storage, while DGAT2 is responsible for the balance of basic fat in various tissues (*36-38*). The high expression of *DGAT2* in the apical turn may be responsible for the abundance of LDs from the apical turn and needs to be further confirmed.

4.2. Apical Hensen's cells may have a better response to the stimulation

Individuals with sensorineural hearing loss, including HHL, NIHL, and ARHL, usually experience a decrease in high-frequency hearing at first (*39-43*). Hearing loss usually begins as high-frequency hearing loss (*39-44*). For example, in conditions such as NIHL, high-frequency hearing is the first to decline after stimulus onset; high-frequency hearing thresholds also recover more slowly after stimulus disappearance (*41,44*). This suggests that cells in different parts of the cochlea usually have different survival abilities and differ in their recoverability from stimulation.

The reasons for high-frequency vulnerability remain unclear, potentially relating to diverse factors. This vulnerability may be attributed to various cells, such as HCs, SCs, spiral ganglion cells, and other cochlear cells. For the hair cells, such as IHCs, their ability to recover in response to stimuli may differ. For instance, the protective genes *PRKD1* and *SNCG*, associated with IHC survival, exhibited upregulation at the apical turn. Conversely, the negative regulatory genes *NME2* and *FBXO32* manifested upregulation at the basal turns (*26*). Basal HCs demonstrate reduced tolerance to oxygen free radicals, increasing their susceptibility to apoptosis (*44*). Sensory neuron cells exhibit molecular variations across the subtypes of spiral ganglion neurons on the tonotopic axis. Genes such as *LRRC52*, *KCNIP4*, *ANXA5*, and *RYR3*, relevant to functionality, displayed regional differences (*27*). Considering the crucial role of Hensen's cells in maintaining the auditory epithelium's integrity, it is important to also examine their function in high-frequency vulnerability (basal turn).

There was not just a morphological difference between the Hensen's cells from apical and basal turns. These cells exhibit significant differences in genetic expression, particularly within pathways related to

energy and lipid metabolism, which correlate with their morphological characteristics. Hensen's cells are dynamic entities actively involved in lipid and energy homeostasis. We proposed that apical Hensen's cells may have enhanced capacities for energy storage and metabolic processing, involving intricate processes such as oxidation and peroxide transport. Such features could potentially contribute to the recovery and maintenance of the organ of Corti function following environmental stimulation. Notably, the GO term "response to decreased oxygen levels" was enriched. This kind of response is critical for cochlear cell survival under oxygen-deprived environments, which could be indicative of the difference in resilience and adaptability between cells in the apical and basal turn. Simultaneously, the KEGG pathway enrichment for "Platinum drug resistance" suggested that these cells may possess enhanced mechanisms for dealing with the cytotoxic effects of platinum-based chemotherapeutic agents. This could reflect a sophisticated network of genes involved in DNA repair, and apoptosis regulation, endowing the Hensen's cells with the capacity to survive and maintain function during drug exposure.

4.3. Many SNHL-associated gene mutations are expressed at low levels in Hensen's cells at the basal turn, leading to clinical hearing loss in high-frequency

Cochlear function is influenced by both genetic and environmental factors. A significant number of deafness-causing genes are mainly expressed in SCs (*45*), and deafness genes are the most important factors causing HHL (*46,47*), especially *GJB2, GJB3,* and *SLC26A4*, which have a high carriage rate (*1,48-50*). Under specific circumstances, the gene expression patterns observed in the basal turn of the cochlea may contribute to greater challenges in maintaining normal cochlear function. This can cause a more rapid decline below a critical threshold when the gene loses its function compared to that in the apical turn. This disparity arises due to a gene expression gradient that is more pronounced in the basal turn, leading to early progressive loss of high-frequency hearing (*51*). Investigating the SCs across various turns can enhance our understanding of the pathology associated with specific-frequency hearing loss.

In Hensen's cells, we analyzed the susceptibility genes for HHL, NIHL, and ARHL at different turns. Notably, certain genes demonstrated significant differences in their expression levels, as indicated in Tables 1, 2, and 3. *GJB2*, *GJB6,* and *P2RX2* are all associated with HHL, NIHL, and ARHL. Mutations in *GJB2* significantly contribute to non-syndromic deafness, representing nearly half of all moderate-to-profound congenital cases. *GJB2* can either form a homomeric gap junction on its own or a heteromeric gap junction in conjunction with *GJB6*. Our research indicates a higher expression of *GJB2* and *GJB6* at the apical turn (high-frequency region), aligning with findings from previous studies (*52*).

P2RX2, also known as Purinergic Receptor *P2X2*, plays a pivotal role in several auditory processes. This includes regulating sound transduction, auditory neurotransmission, outer hair cell electromotility, and inner ear gap junctions. Additionally, it mediates K+ recycling and facilitates synaptic transmission between neurons and smooth muscles (*53*). Patients harboring mutations in *P2RX2* can experience progressive hearing loss accompanied by heightened noise sensitivity. Notably, *P2RX2* expression has been observed to decline with age (*21*). Studies conducted with animal models have found that noise can reduce sound transduction and synaptic transmission between HCs by increasing ATP levels and thus activating *P2X2* receptors and reducing *P2RX2* receptor-mediated regulation of endocochlear potential in the aging mouse cochlea resulting in hearing sensitivity impairment (*54,55*).

Our comprehensive analysis has shown that Hensen's cells display significant morphological variations that reflect their different energy storage and metabolic capabilities. The data demonstrated that Hensen's cells from different cochlear turns exhibit pronounced disparities in lipid metabolism, oxidative capacity, and gene expression that are consistent with their morphological characteristics. It appears that Hensen's cells from the basal turn (high-frequency region) may have reduced resilience to environmental challenges such as acoustic trauma and ototoxic agents. This compromised metabolic functionality could lead to an inadequate energy supply to sensory cells, culminating in damage or death of hair cells near the basal turn. Genes such as *GJB2, GJB6*, and *P2RX2* show variable expression along the cochlear axis, which may be clinically critical in initiating cochlear dysfunction and subsequent high-frequency hearing loss. This study emphasized the significance of conducting a thorough investigation of supporting cells to gain a better understanding of the complex physiology of the cochlea and to identify effective measures for preserving high-frequency hearing.

Acknowledgements

We sincerely appreciate the guidance of our tutors and every member of our team.

Funding: This work was supported by the National Natural Science Foundation of China (grant numbers 81870730, 82071064), and the Capital's Funds for Health Improvement and Research (grant number, CFH 2022-2-1092).

Conflict of Interest: The authors have no conflicts of interest to disclose.

References

1. Cederholm JME, Ryan AF, Housley GD. Onset kinetics of noise-induced purinergic adaptation of the 'cochlear amplifier.' Purinergic Signal. 2019; 15:343-355.
2. Waldhaus J, Durruthy-Durruthy R, Heller S. Quantitative High-Resolution Cellular Map of the Organ of Corti. Cell Rep. 2015; 11:1385-1399.
3. Scheffer DI, Shen J, Corey DP, Chen ZY. Gene Expression by Mouse Inner Ear Hair Cells during Development. J Neurosci. 2015; 35:6366-6380.
4. Monzack EL, Cunningham LL. Lead roles for supporting actors: critical functions of inner ear supporting cells. Hear Res. 2013; 303:20-29.
5. Wan G, Corfas G, Stone JS. Inner ear supporting cells: Rethinking the silent majority. Semin Cell Dev Biol. 2013; 24:448-459.
6. Raica M. A short story of Victor Hensen and a cell of the internal ear. Published online. 2012:3.
7. Spicer SS, Schulte BA. Differences along the place-frequency map in the structure of supporting cells in the gerbil cochlea. Hear Res. 1994; 79:161-177.
8. Spicer SS, Schulte BA. The fine structure of spiral ligament cells relates to ion return to the stria and varies with place frequency. Hear Res. 1996; 100:80-100.
9. Sugasawa M, Erostegui C, Blanchet C, Dulon D. ATP activates a cation conductance and Ca^{2+}-dependent Cl^- conductance in Hensen cells of guinea pig cochlea. Am J Physiol. 1996; 271:C1817-1827.
10. Fechner FP, Nadol JB JR, Burgess BJ, Brown MC. Innervation of supporting cells in the apical turns of the guinea pig cochlea is from type II afferent fibers. J Comp Neurol. 2001; 429:289-298.
11. Urrutia RA, Kalinec F. Biology and Pathobiology of Lipid Droplets and their Potential Role in the Protection of the Organ of Corti. Hear Res. 2015; 330(Pt A):26-38.
12. Zhao HB, Liu LM, Yu N, Zhu Y, Mei L, Chen J, Liang C. Efferent neurons control hearing sensitivity and protect hearing from noise through the regulation of gap junctions between cochlear supporting cells. J Neurophysiol. 2022; 127:313-327.
13. Picelli S, Faridani OR, Björklund AK, Winberg G, Sagasser S, Sandberg R. Full-length RNA-seq from single cells using Smart-seq2. Nat Protoc. 2014; 9:171-181.
14. Picelli S, Björklund ÅK, Faridani OR, Sagasser S, Winberg G, Sandberg R. Smart-seq2 for sensitive full-length transcriptome profiling in single cells. Nat Methods. 2013; 10:1096-1098.
15. Nishio SY, Hattori M, Moteki H, Tsukada K, Miyagawa M, Naito T, Yoshimura H, Iwasa Y, Mori K, Shima Y, Sakuma N, Usami S. Gene expression profiles of the cochlea and vestibular endorgans: localization and function of genes causing deafness. Ann Otol Rhinol Laryngol. 2015; 124 Suppl 1:6S-48S.
16. Chen XM, Xue XM, Yu N, Guo WW, Yuan SL, Jiang QQ, Yang SM. The Role of Genetic Variants in the Susceptibility of Noise-Induced Hearing Loss. Front Cell Neurosci. 2022; 16:946206.
17. Xu K, Chen S, Xie L, Qiu Y, Bai X, Liu XZ, Zhang HM, Wang XH, Jin Y, Sun Y, Kong WJ. Local Macrophage-Related Immune Response Is Involved in Cochlear Epithelial Damage in Distinct Gjb2-Related Hereditary Deafness Models. Front Cell Dev Biol. 2021; 8:597769.
18. Trebusak Podkrajsek K, Tesovnik T, Bozanic Urbancic N, Battelino S.. Novel *GRHL2* Gene Variant Associated with Hearing Loss: A Case Report and Review of the Literature. Genes. 2021; 12:484.
19. Wells HRR, Newman TA, Williams FMK. Genetics of age-related hearing loss. J Neurosci Res. 2020; 98:1698-1704.
20. Di Stazio M, Morgan A, Brumat M, Bassani S, Dell'Orco D, Marino V, Garagnani P, Giuliani C, Gasparini P, Girotto G. New age-related hearing loss candidate genes in humans: an ongoing challenge. Gene. 2020; 742:144561.
21. Bouzid A, Smeti I, Dhouib L, Roche M, Achour I, Khalfallah A, Gibriel AA, Charfeddine I, Ayadi H, Lachuer J, Ghorbel A, Petit C, Masmoudi S. Down-expression of *P2RX2*, *KCNQ5*, *ERBB3* and *SOCS3* through DNA hypermethylation in elderly women with presbycusis. Biomarkers. 2018; 23:347-356.
22. Haider HF, Flook M, Aparicio M, Ribeiro D, Antunes M, Szczepek AJ, Hoare DJ, Fialho G, Paço JC, Caria H. Biomarkers of Presbycusis and Tinnitus in a Portuguese Older Population. Front Aging Neurosci. 2017; 9:346.
23. Xu Z, Tu S, Pass C, Zhang Y, Liu H, Diers J, Fu Y, He DZZ, Zuo J. Profiling mouse cochlear cell maturation using 10× Genomics single-cell transcriptomics. Front Cell Neurosci. 2022; 16:962106.
24. Langlie J, Finberg A, Bencie NB, Mittal J, Omidian H, Omidi Y, Mittal R, Eshraghi AA. Recent advancements in cell-based models for auditory disorders. BioImpacts BI. 2022; 12:155-169.
25. Hoa M, Olszewski R, Li X, Taukulis I, Gu S, DeTorres A, Lopez IA, Linthicum FH Jr, Ishiyama A, Martin D, Morell RJ, Kelley MW. Characterizing Adult Cochlear Supporting Cell Transcriptional Diversity Using Single-Cell RNA-Seq: Validation in the Adult Mouse and Translational Implications for the Adult Human Cochlea. Front Mol Neurosci. 2020; 13:13.
26. Tang F, Chen X, Jia L, Li H, Li J, Yuan W. Differential Gene Expression Patterns Between Apical and Basal Inner Hair Cells Revealed by RNA-Seq. Front Mol Neurosci. 2020; 12:332.
27. Shrestha BR, Chia C, Wu L, Kujawa SG, Liberman MC, Goodrich LV. Sensory neuron diversity in the inner ear is shaped by activity. Cell. 2018; 174:1229-1246.e17.
28. Liu H, Pecka JL, Zhang Q, Soukup GA, Beisel KW, He DZ.. Characterization of Transcriptomes of Cochlear Inner and Outer Hair Cells. J Neurosci. 2014; 34:11085-11095.
29. Olzmann JA, Carvalho P. Dynamics and functions of lipid droplets. Nat Rev Mol Cell Biol. 2019; 20:137-155.
30. Walther TC, Chung J, Farese RV. Lipid Droplet Biogenesis. Annu Rev Cell Dev Biol. 2017; 33:491-510.
31. Engstrom H, Wersall J. Is there a special nutritive cellular system around the hair cells in the organ of Corti. Ann Otol Rhinol Laryngol. 1953; 62:507-512.
32. Zhao LD, Liu J, Hu YY, Sun JH, Yang SM. Supporting Cells–a New Area in Cochlear Physiology Study. J Otol. 2008; 3:9-17.
33. Merchan MA, Merchan JA, Ludeña MD. Morphology of Hensen's cells. J Anat. 1980; 131(Pt 3):519-523.
34. del Cañizo Alvarez A, Merchán Cifuentes MA. A possible function of Hensen cells of the internal ear in the guinea pig. An Otorrinolaringol Ibero-Am. 1986; 13:627-638.
35. del Cañizo-Alvarez A, Merchan-Cifuentes MA, Arevalo M. Changes induced by sonic stimulation in the cells of Hensen of the inner ear. Rev Laryngol - Otol - Rhinol. 1987; 108:327-329.
36. Chen G, Harwood JL, Lemieux MJ, Stone SJ, Weselake RJ. Acyl-CoA:diacylglycerol acyltransferase: Properties,

physiological roles, metabolic engineering and intentional control. Prog Lipid Res. 2022; 88:101181.
37. Bhatt-Wessel B, Jordan TW, Miller JH, Peng L. Role of *DGAT* enzymes in triacylglycerol metabolism. Arch Biochem Biophys. 2018; 655:1-11.
38. Liu Q, Siloto RM, Lehner R, Stone SJ, Weselake RJ. Acyl-CoA:diacylglycerol acyltransferase: molecular biology, biochemistry and biotechnology. Prog Lipid Res. 2012; 51:350-377.
39. Fetoni AR, Pisani A, Rolesi R, Paciello F, Viziano A, Moleti A, Sisto R, Troiani D, Paludetti G, Grassi C. Early Noise-Induced Hearing Loss Accelerates Presbycusis Altering Aging Processes in the Cochlea. Front Aging Neurosci. 2022; 14:803973.
40. Cunningham LL, Tucci DL. Hearing Loss in Adults. N Engl J Med. 2017; 377:2465-2473.
41. Kurabi A, Keithley EM, Housley GD, Ryan AF, Wong AC. Cellular mechanisms of noise-induced hearing loss. Hear Res. 2017; 349:129-137.
42. Ding D, Jiang H, Salvi RJ. Mechanisms of Rapid Sensory Hair-Cell Death Following Co-administration of Gentamicin and Ethacrynic Acid. Hear Res. 2010; 259:16.
43. Ou HC, Bohne BA, Harding GW. Noise damage in the C57BL/CBA mouse cochlea. Hear Res. 2000; 145:111-122.
44. Sha SH, Taylor R, Forge A, Schacht J. Differential vulnerability of basal and apical hair cells is based on intrinsic susceptibility to free radicals. Hear Res. 2001; 155:1-8.
45. Usami SI, Nishio SY, Moteki H, Miyagawa M, Yoshimura H. Cochlear Implantation from the Perspective of Genetic Background. Anat Rec Hoboken. 2020; 303:563-593.
46. Lieu JEC, Kenna M, Anne S, Davidson L. Hearing Loss in Children: A Review. JAMA. 2020; 324:2195.
47. Richardson GP, de Monvel JB, Petit C. How the Genetics of Deafness Illuminates Auditory Physiology. Annu Rev Physiol. 2011; 73:311-334.
48. Dai P, Huang LH, Wang GJ, *et al*. Concurrent Hearing and Genetic Screening of 180,469 Neonates with Follow-up in Beijing, China. Am J Hum Genet. 2019; 105:803-812.
49. Wang QJ, Zhao YL, Rao SQ, Guo YF, Yuan H, Zong L, Guan J, Xu BC, Wang DY, Han MK, Lan L, Zhai SQ, Shen Y. A distinct spectrum of SLC26A4 mutations in patients with enlarged vestibular aqueduct in China. Clin Genet. 2007; 72:245-254.
50. Xia J, Liu C, Tang B, *et al*. Mutations in the gene encoding gap junction protein β-3 associated with autosomal dominant hearing impairment. Nat Genet. 1998; 20:370-373.
51. Yoshimura H, Takumi Y, Nishio S ya, Suzuki N, Iwasa Y ichiro, Usami S ichi. Deafness Gene Expression Patterns in the Mouse Cochlea Found by Microarray Analysis. PLoS ONE. 2014; 9:e92547.
52. Zhao HB, Yu N. Distinct and gradient distributions of connexin26 and connexin30 in the cochlear sensory epithelium of guinea pigs. J Comp Neurol. 2006; 499:506-518.
53. Morton-Jones RT, Vlajkovic SM, Thorne PR, Cockayne DA, Ryan AF, Housley GD. Properties of ATP-gated ion channels assembled from *P2X2* subunits in mouse cochlear Reissner's membrane epithelial cells. Purinergic Signal. 2015; 11:551-560.
54. Yan D, Zhu Y, Walsh T, *et al*. Mutation of the ATP-gated *P2X2* receptor leads to progressive hearing loss and increased susceptibility to noise. Proc Natl Acad Sci U S A. 2013; 110:2228-2233.
55. Telang RS, Paramananthasivam V, Vlajkovic SM, Munoz DJ, Housley GD, Thorne PR.. Reduced $P2x_2$ receptor-mediated regulation of endocochlear potential in the ageing mouse cochlea. Purinergic Signal. 2010; 6:263-272.

Received March 4, 2024; Revised March 29, 2024; Accepted April 3, 2024.

**Address correspondence to:*
Lihui Huang, Otolaryngology Head and Neck Surgery, Beijing Tongren Hospital, Capital Medical University, Beijing 100730, China; Beijing Institute of Otolaryngology, Beijing 100005, China; Key Laboratory of Otolaryngology Head and Neck Surgery, Ministry of Education, Beijing 100005, China.
E-mail: huanglihui@ccmu.edu.cn

Ning Yu, College of Otolaryngology Head and Neck Surgery, Chinese PLA General Hospital, Beijing 100853, China; National Clinical Research Center for Otolaryngologic Diseases, Beijing 100853, China.
E-mail: yuning@301hospital.org

Released online in J-STAGE as advance publication April 5, 2024.